



ARTICLE

Received 27 Apr 2016 | Accepted 8 Jun 2016 | Published 7 Jul 2016

DOI: [10.1038/ncomms12168](https://doi.org/10.1038/ncomms12168)

OPEN

Van der Waals pressure and its effect on trapped interlayer molecules

K.S. Vasu¹, E. Prestat², J. Abraham¹, J. Dix³, R.J. Kashtiban⁴, J. Beheshtian⁵, J. Sloan⁴, P. Carbone³, M. Neek-Amal⁵, S.J. Haigh², A.K. Geim¹ & R.R. Nair¹

Van der Waals assembly of two-dimensional crystals continue attract intense interest due to the prospect of designing novel materials with on-demand properties. One of the unique features of this technology is the possibility of trapping molecules between two-dimensional crystals. The trapped molecules are predicted to experience pressures as high as 1 GPa. Here we report measurements of this interfacial pressure by capturing pressure-sensitive molecules and studying their structural and conformational changes. Pressures of 1.2 ± 0.3 GPa are found using Raman spectrometry for molecular layers of 1-nm in thickness. We further show that this pressure can induce chemical reactions, and several trapped salts are found to react with water at room temperature, leading to two-dimensional crystals of the corresponding oxides. This pressure and its effect should be taken into account in studies of van der Waals heterostructures and can also be exploited to modify materials confined at the atomic interfaces.

¹School of Physics and Astronomy, University of Manchester, Manchester M13 9PL, UK. ²School of Materials, University of Manchester, Manchester M13 9PL, UK. ³School of Chemical Engineering and Analytical Science, University of Manchester, Manchester M13 9PL, UK. ⁴Department of Physics, University of Warwick, Coventry CV4 7AL, UK. ⁵Department of Physics, Shahid Rajaee Teacher Training University, 16875-163, Lavizan, Tehran, Iran. Correspondence and requests for materials should be addressed to R.R.N. (email: rahul@manchester.ac.uk).

Van der Waals (vdW) interactions play a critical role in numerous phenomena and applications such as catalysis, adhesion, lubrication, nanofluidics and fabrication of novel vdW materials^{1–10}. In the latter case, two-dimensional (2D) crystals assembled layer by layer are kept together only by vdW forces^{1,11}. Various heterostructures composed of graphene, BN, MoS₂ and so on have been intensively investigated and already shown potential for a wide range of electronic and optical applications^{3,4}. During the fabrication of such heterostructures, molecules become trapped between 2D crystals, which results in enclosures of nanometre height⁵. Such nano-enclosures were also fabricated intentionally, mostly using graphene, to serve as hydrothermal reactors^{12,13}, visualize chemical processes^{14,15} and for electron and atomic force microscopy (AFM) of biological samples and adlayers^{6,16,17}. Hydrothermal reactions reported inside the graphene nanobubbles were limited to the pressure created at high temperatures, where trapped solvents and molecules reach their critical or super critical phase to initiate the chemical reactions similar to the conventional hydrothermal anvil cell¹³. When nano-enclosures are created at room temperature, a pressure P builds up, and it can be extremely high due to an exceptionally high stiffness of graphene and the fact that vdW forces become extremely strong on a sub-nanometre scale. The value of P is determined by a balance between the resulting hydrostatic pressure, the deformation energy of 2D crystals and a gain in the adhesion energy^{6,18}. The deformation energy favours enclosures with a flat top. In the first approximation, the pressure can be estimated as $\approx E_w/h$, where E_w is the adhesion energy and h is the height of the nano-enclosure^{6,18}. For a trapped monolayer, this estimate yields P of the order of 1 GPa, in agreement with further rigorous analysis^{7,18,19}. However, such large vdW pressure has never been measured experimentally, nor has its effect on physical, structural and chemical properties of entrapped molecules been studied.

Here we demonstrate the existence of the huge vdW pressure inside the nano-enclosures made from 2D crystals by studying changes in Raman spectra of pressure-sensitive molecules such as triphenyl amine (TPA) and boric acid (BA). We also report the effect of vdW pressure on the chemistry of materials inside nano-enclosures by investigating the chemical stability of trapped compounds [MgCl₂, CsI, CuSO₄ and Ca(OH)₂] using both Raman spectroscopy and transmission electron microscopy (TEM).

Results

Fabrication of nano-enclosures. Various 2D crystals have been used in our experiments to prepare nano-enclosures as described in detail in the Methods and Supplementary Fig. 1. For brevity, we focus below on enclosures made from an archetypal 2D material, graphene. Graphene-encapsulated (GE) molecule/salt structures were prepared by drop casting a small amount (2 μ l) of a dilute (≤ 0.1 M) molecular or salt solution onto a graphene layer. A second (top) graphene crystal was then carefully placed on top using the standard transfer techniques^{1,3} to trap the solution. We normally used few-layer graphene as a bottom layer to minimize its crumpling during the drop casting. The liquid between graphene crystals was allowed to dry overnight at room temperature and then further dried in a vacuum desiccator. As a result, the two graphene layers strongly attached to each other with a tiny amount of the solution being captured in between.

vdW pressure measurements. Figure 1a shows an optical image of one of our GE-TPA samples. One can see many small bubbles (indicated with arrows in Fig. 1a) within seemingly featureless areas. However, AFM reveals that these areas are actually composed of flat nano-enclosures with a height of ≈ 1 nm (region 1 in the inset of Fig. 1a), which are surrounded by numerous submicron bubbles of several nanometres in height (region 2). Such 1-nm-thick flat regions are found to be continuous, and their lateral size can be as large as several micrometres. A similar AFM landscape was found for GE-BA samples (Supplementary Note 1 and Supplementary Fig. 2a).

To determine the pressure inside this type of graphene nano-enclosure, we perform Raman spectroscopy. Figure 1b compares spectra obtained from a bubble of several microns in size and from a flat 1-nm-thick region. The Raman spectrum for bubble agrees with the known spectrum of bulk TPA²⁰ where the major Raman bands are centred at ≈ 997 cm⁻¹ due to C–C stretching accompanied by weak C–N stretching, 1,025 cm⁻¹ due to C–N stretching with associated C–C stretching and 1,172 cm⁻¹ due to combined C–N and C–C stretching. In stark contrast, the Raman spectrum of flat GE-TPA regions show all the bands being blueshifted with peaks appearing at $\approx 1,011$, 1,040 and 1,195 cm⁻¹, respectively. The widths of these bands are larger than those of bulk TPA. The observed changes in the Raman bands of captured TPA molecules are attributed to structural

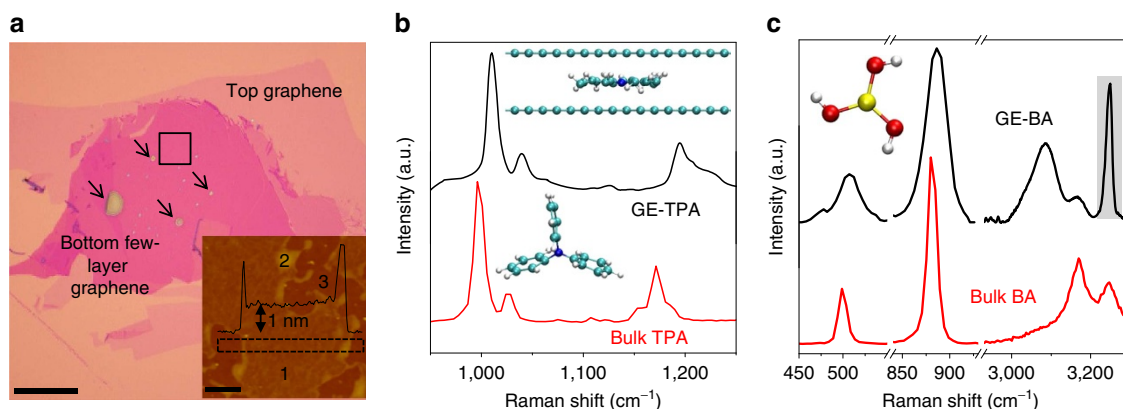


Figure 1 | Probing vdW pressure by Raman spectroscopy. (a) Optical micrograph of a graphene-encapsulated TPA on few-layer graphene placed on an oxidized Si wafer. Scale bar, 30 μ m. Arrows indicate some of the small bubbles in the sample. Inset: AFM image of the region indicated by the square in **a**. A 1-nm-thick flat region is marked as 1, one of many small bubbles marked as 2 and the region in which top and bottom graphene are attached as 3. Scale bar, 1 μ m. Black curve: height profile along the dotted rectangle. (b) Typical Raman spectra (514-nm excitation) from macroscopic bubbles and regions such as 1. The bottom inset shows the standard molecular structure of TPA. Top inset: modified structure of TPA between graphene sheets as found in MD simulations. (c) Raman spectra (514-nm excitation) of bulk BA and GE-BA. Inset: molecular structure of BA. The shaded area indicates the 2D' band of graphene.

changes because of the confinement of TPA between graphene layers (Fig. 1b). Indeed, the propeller-shaped structure of TPA makes it highly sensitive to the uniaxial confinement, which can be translated into uniaxial pressure on the molecule. The observed Raman changes are in good agreement with those found for TPA at high pressures using conventional measurements in diamond anvil cells²¹. Comparison of our results with the latter measurements allows an estimate of P inside our flat graphene nano-enclosures as 1–1.5 GPa. To support this conclusion, we have also performed molecular dynamic simulations for TPA confined in a graphene capillary. They show that TPA molecules undergo a conformational change (from the propeller to planar structure; inset in Fig. 1b), if the separation between graphene sheets decreases below 1 nm (Supplementary Note 2 and Supplementary Figs 3–5).

Similar experiments were performed with boric acid. Unlike TPA, BA molecules have a nearly planar structure already at ambient pressure. They are attracted to each other by hydrogen bonding and organize layered structures²². Figure 1c shows Raman spectra obtained from bulk BA and from a 1-nm-thick enclosure with BA. The main bands for bulk BA are at 500 cm^{-1} that corresponds to O–B–O angle deformation, 880 cm^{-1} for B–O stretching, $3,167\text{ cm}^{-1}$ for symmetric O–H stretching and $3,245\text{ cm}^{-1}$ for antisymmetric O–H stretching²³. For 1-nm-thick encapsulated BA, the two B–O modes exhibit broadening and a blueshift (509 and 885.5 cm^{-1} , respectively), whereas the O–H stretching modes show a redshift and a notable change in the shape of the peaks (Fig. 1c). Similar to the case of TPA, the observed changes in the Raman spectrum of flat GE-BA are consistent with previously reported hydrostatically pressurized BA²³. Distinct from the other Raman bands of BA, the redshift for O–H stretching vibrations under pressure can be attributed to shortening of the hydrogen bond, which leads to lengthening and weakening of the parent O–H bond under compression²⁴. The structure of BA is highly sensitive to pressure so that the O–B–O deformation and symmetric B–O stretching modes shift by 7.0 and 4.5 cm^{-1} per GPa, respectively²³. This allows us to estimate the pressure inside our 1-nm-thick graphene enclosures as 1.2 ± 0.3 GPa, in good agreement with the vdW pressure measured for TPA. Besides probing the vdW pressure, Raman spectroscopy also allowed us to estimate the strain developed in top-layer graphene during the BA/TPA

encapsulation by analysing the shift in peak position of graphene G and 2D bands (Supplementary Note 3 and Supplementary Fig. 6).

Effects of vdW pressure on trapped salts. The extremely high vdW pressure acting on substances captured between 2D crystals cannot be ignored and may modify physical and chemical properties of both trapped compounds and confining crystals experiencing the same pressure. As an example, we show that compounds such as MgCl_2 , CuSO_4 and $\text{Ca}(\text{OH})_2$ become reactive with water at room temperature under the pressure inside nano-enclosures. Figure 2a shows an AFM image of MgCl_2 solution trapped between graphene layers (Supplementary Note 1 and Supplementary Fig. 2b,c). Similar to the case of trapped TPA and BA, GE- MgCl_2 samples contain numerous flat regions with $h \approx 1\text{ nm}$. Figure 2b plots typical Raman spectra acquired from such regions for 0.1 M solutions of MgCl_2 in water and methanol. As a reference, we also provide Raman spectra from an anhydrous MgCl_2 powder and a region where a large droplet of 0.1 M aqueous solution of MgCl_2 was allowed to dry up on top of graphene outside the nano-enclosures.

Anhydrous MgCl_2 exhibits two Raman bands, one at $\approx 240\text{ cm}^{-1}$ due to out-of-plane vibrations and another at $\approx 157\text{ cm}^{-1}$ assigned to in-plane phonons²⁵. Also, the Raman spectrum obtained from the dried MgCl_2 solution shows typical signatures of hydrated MgCl_2 (ref. 26; Supplementary Note 4 and Supplementary Fig. 7) with a broad redshifted peak at $\approx 200\text{ cm}^{-1}$. In contrast, the Raman spectrum of 0.1 M aqueous MgCl_2 inside the flat GE region does not show any of the expected features but instead a sharp peak appears at $125 \pm 3\text{ cm}^{-1}$. This new Raman band was universally observed for many flat encapsulated regions, reaching several microns in size. In addition to the 125 cm^{-1} band, we also observe changes in the Raman spectrum of graphene covering MgCl_2 regions, which include the emergence of the D peak (Supplementary Note 5 and Supplementary Fig. 8). In comparison, nano-enclosures with MgCl_2 dissolved in methanol show only broadened Raman signature characteristic of anhydrous MgCl_2 and no sign of the 125 cm^{-1} peak (Fig. 2b).

Although the described spectroscopic changes indicate marked changes in the structure of the trapped aqueous MgCl_2 , Raman spectroscopy is unable to reveal what kind of transformation

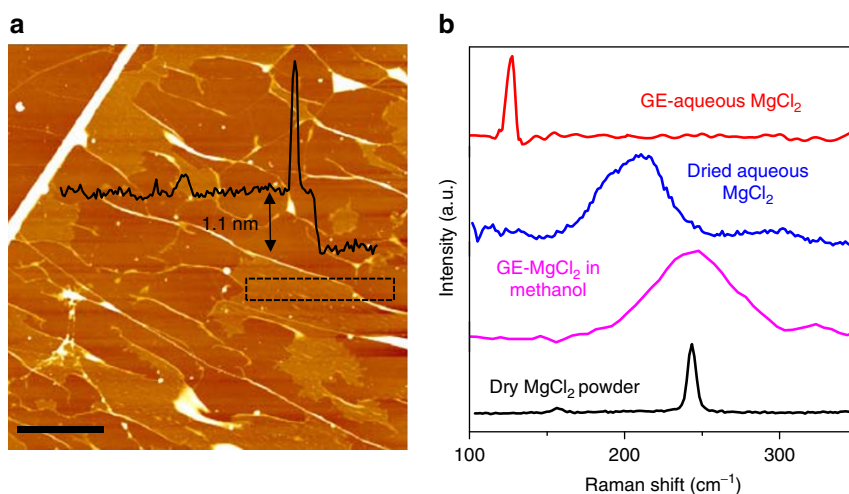


Figure 2 | Encapsulation-induced chemical reactions. (a) AFM image obtained from graphene-encapsulated aqueous MgCl_2 . Scale bar, $2\text{ }\mu\text{m}$. Nanometre-thick flat regions are clearly seen being separated by wrinkles and occasional bubbles of triangular and arbitrary shapes. Black curve: height profile along the dotted rectangle. (b) Raman spectra (488 nm excitation) measured from flat regions encapsulating MgCl_2 dissolved in water and methanol. For comparison, spectra for anhydrous and hydrated MgCl_2 are shown.

takes place. To elucidate this, we have performed TEM analysis of constituents inside the nano-enclosures (see Methods). Our low-magnification TEM images confirm that the samples contain flat enclosed areas with only a few small bubbles in between (inset of Fig. 3a), in agreement with our AFM imaging. Elemental analysis using energy dispersive X-ray (EDX) spectroscopy shows that the bubbles contain magnesium, oxygen and chlorine, as expected for aqueous MgCl_2 , whereas the flat enclosures contain magnesium and oxygen but surprisingly with no signature of chlorine (Fig. 3b). High-resolution TEM also reveals that the flat regions are thin crystallites of one to few layers in thickness, which have a square lattice with lattice constant of $2.1 \pm 0.05 \text{ \AA}$ (Fig. 3a). Electron diffraction and electron energy loss spectroscopy (EELS) analyses confirm that these nanocrystals are MgO, with the EELS oxygen K-edge from the enclosed material showing a good match to the reference spectrum for bulk MgO (Fig. 3c). Furthermore, fast Fourier transform of high-resolution image of the thinnest MgO crystallites show the presence of a (110) lattice reflection, and our simulated electron diffraction patterns confirm that such (110) reflections are a clear signature of monolayer MgO (Supplementary Note 6 and Supplementary Figs 9 and 10). All this unequivocally shows that the observed nanocrystals inside graphene nano-enclosures are MgO. This conclusion is also consistent with the observed 125 cm^{-1} Raman band that was previously reported for MgO crystals^{27,28}.

Discussion

We have performed similar experiments with aqueous solutions of other compounds including CuSO_4 , CsI and $\text{Ca}(\text{OH})_2$ (Supplementary Note 7 and Supplementary Figs 11 and 12). Similar to the case of MgCl_2 , our Raman and TEM analyses show that graphene-encapsulated CuSO_4 and $\text{Ca}(\text{OH})_2$ are converted into CuO and CaO, respectively, whereas graphene-encapsulated CsI remains stable. This agrees with our density functional theory calculations performed for MgCl_2 , $\text{Mg}(\text{OH})_2$ and CsI trapped with water inside a hydrophobic cage (Supplementary Note 8 and Supplementary Fig. 13). They suggest the formation of a Mg–O

bond in the case of MgCl_2 and $\text{Mg}(\text{OH})_2$, and no changes for CsI. Although the calculations do not elucidate the underlying mechanism for the room-temperature reactivity of the salts with H_2O , it is reasonable to assume that the reactions are induced by the high vdW pressure. Indeed, the probability of ionization of water molecules strongly increases with increasing P , and changes in pressure from 0.1 MPa to 1 GPa are known to cause the ionization constant of water to change by two orders of magnitude²⁹, thus favouring the hydrolysis. We propose that the observed room-temperature reaction of nano-enclosed salts with water involves the pressure-assisted hydrolysis of salts into their hydroxides followed by decomposition to the corresponding oxides (Supplementary Note 9). Similar vdW pressure-assisted reactions were also observed in other 2D crystal nano-enclosures such as BN (Supplementary Note 10 and Supplementary Fig. 14). Conversion of bulk salts to corresponding hydroxides or oxides was only observed previously at high temperatures and pressures³⁰, and we assume that the confinement and pressure has a significant influence on the feasibility of observed reaction at room temperature. The effect of confinement apparently brings the close proximity of metal ions to ionized water molecules to begin hydrolysis reaction and it is important to note that without the vdW confinement the pressure alone could not make the observed reaction feasible at room temperature^{31,32}. The reaction byproducts such as HCl and water are probably accumulated in the small bubbles and wrinkles observed in the flat encapsulated regions (Supplementary Fig. 2b) or evaporated through microscopic defects created in graphene during the reaction as the presence of graphene's D peak indicates (Supplementary Note 5 and Supplementary Fig. 8). The proposed mechanism is also consistent with the absence of changes for CsI. In this case, the salt of strong acid and strong base completely ionizes in water rather than undergoing hydrolysis³³. In contrast, MgCl_2 and CuSO_4 are examples of salts of a weak base and strong acid that normally undergo hydrolysis. The observed non-reactivity for MgCl_2 in methanol is naturally explained by the absence of water. Still, further experimental and theoretical studies are needed for a better understanding of the chemical transformations inside graphene nano-enclosures.

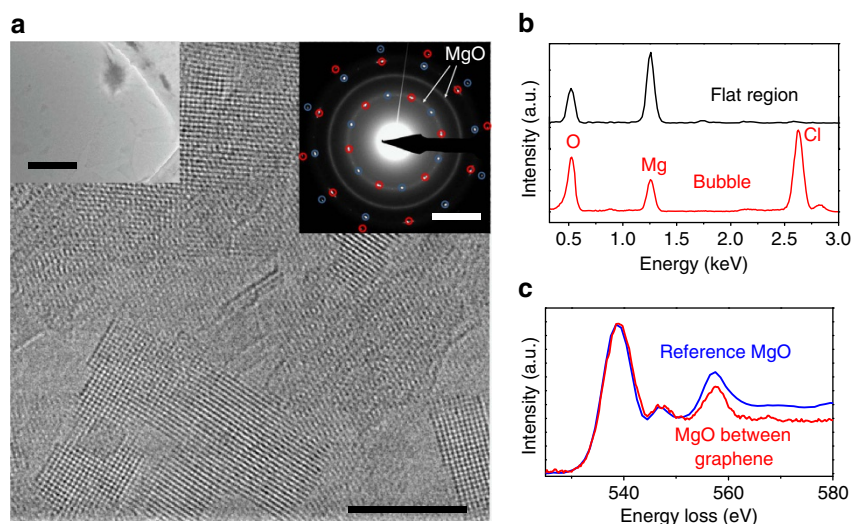


Figure 3 | TEM on graphene-encapsulated aqueous MgCl_2 . (a) High-resolution TEM image of MgO nanocrystal formed between two graphene layers. Scale bar, 5 nm. Inset on left of panel: low-magnification TEM image showing flat encapsulated regions and a larger bubble. Scale bar, 500 nm. Inset on right of panel: diffraction pattern taken from a 1- μm -diameter flat area shows two hexagonal patterns (red and blue circles), which come from the top and bottom graphene layers, and additional diffraction rings corresponding to the {200} and {220} planes of polycrystalline MgO. Scale bar, 5 nm^{-1} . (b) EDX spectra from a flat encapsulated region and from a large bubble. (c) Oxygen-K edge spectrum from nanocrystals such as in **a** compared with the spectrum of bulk MgO from the EELS database (<https://eelsdb.eu/spectra/magnesium-oxide-2>).

In conclusion, our work shows that huge pressures are exerted on materials trapped at interfaces during assembly of vdW heterostructure and that these pressures can lead to unexpected physical and chemical changes. This should be considered in analysis of the properties of vdW heterostructures, especially because the neighbouring 2D crystals experience the same pressure. Our results can be exploited to induce novel physical phenomena in nano-enclosures and create new chemical compounds, which all points at many opportunities to explore the science of nanoconfined materials.

Methods

Fabrication of graphene-encapsulated samples. Graphene-encapsulated samples were prepared by using the wet transfer technique³⁴ to enclose salt or molecule solutions between two micromechanically exfoliated graphene flakes or between a graphene flake and a graphite flake as summarized in Supplementary Fig. 1. Single- and few-layer graphene flakes were prepared on Si/SiO₂ substrates with an oxide thickness of 300 nm using the micromechanical exfoliation³⁵. Optical microscopy was used to locate the graphene flakes of suitable size (50 × 50 μm or above) on Si/SiO₂ substrate (panel 1 in Supplementary Fig. 1) and the thickness of these flakes was verified using Raman spectroscopy³⁶. A thin layer (≈ 200 nm) of A3-950 poly(methyl methacrylate) (PMMA) resist was then spin coated on to a substrate containing the desired flake and subsequently heated at 100 °C for 10 min to evaporate the solvent from the resist (panel 2 in Supplementary Fig. 1). An adhesive tape window was placed above the PMMA layer, ensuring that the desired graphene flake was at the centre of the open area (panel 3 in Supplementary Fig. 1). The tape and PMMA act as a support for the graphene flake allowing it to be lifted away from the Si/SiO₂ substrate. PMMA layer at the periphery of the tape window was then removed to separate the tape window area from the remainder of the PMMA layer. The entire sample was then placed in 3% KOH solution to etch away the SiO₂ layer and thereby separate the graphene flake from the substrate (panel 4 in Supplementary Fig. 1). After this etching process, the tape window with the PMMA layer containing the graphene flake floated on the surface of the KOH solution due to the hydrophobic nature of PMMA, whereas the Si substrate stays at the bottom (panel 5 in Supplementary Fig. 1). Subsequently, the tape window hosting the graphene-PMMA layer was rinsed with deionized water to remove any residual KOH solution. Using the micromanipulation set-up³⁷, this graphene-PMMA layer was carefully placed on top of 2 μl of the molecule or salt solution casted onto the bottom few-layer graphene or graphite flake. We have used 0.001–0.1 M solutions of the molecule or salt, and all reported results were similar even when the different concentrations of molecule or salt solutions were used. All sample solutions were aqueous, except TPA, which is insoluble in water, so methanol was used as the solvent. A single-layer graphene (SLG) has also been tested as a bottom layer but was not ideal as it often ruptured during drop casting of the molecule or salt solution. After placing the single layer of graphene on top of the solution, most of the solution was spontaneously squeezed out by leaving only a very small amount in between the top and bottom graphene layers. The prepared samples were dried overnight at room temperature to let the solvent to evaporate gradually and allow the top graphene layer to collapse onto the bottom graphene flake. These samples were then placed in vacuum (≈ 1 mBar) for several hours to remove any residual solvent and water molecules. Finally, the tape window was detached, and the top PMMA layer was removed using an acetone wash.

Graphene grown using chemical vapour deposition on Cu foil, received from BGT Materials Limited (Manchester, UK), has been used to prepare samples suitable for TEM and scanning TEM high-resolution imaging and analysis. To detach the chemical vapour deposition grown graphene from the Cu foil (5 × 5 mm), the graphene was coated with PMMA and the metal was etched away using a 0.1-M ammonium persulfate aqueous solution. The resulting graphene-PMMA film was then rinsed several times in water and transferred onto a gold mesh Quantifoil TEM support grid. Removal of the PMMA layer was achieved by washing in acetone and isopropyl alcohol baths. The graphene-covered TEM grids produced were then dried in a critical point dryer and subsequently annealed in activated carbon at 250 °C to remove the hydrocarbon contamination³⁸. To prepare the GE salt samples for TEM, salt solution was drop casted at the centre of a graphene-covered TEM grid followed by placing another graphene-covered TEM grid above the droplet. The prepared TEM samples were further dried as described above.

AFM measurements. AFM imaging of the encapsulated samples was performed using a Bruker Dimension FastScan AFM operating in peak force tapping mode.

Raman measurements. A micro Raman set-up consisting of an optical microscope, and a spectrograph with 2,400 and 1,800 lines per mm grating (Reinshaw/Witec spectrometer) was used to obtain Raman spectra in a back-scattering geometry using a × 100 objective lens (numerical aperture = 0.70) under ambient conditions. An Ar-ion multiline tuning laser operating at wavelengths of 488 and 514 nm and a He-Ne laser operating at a wavelength of 633 nm were used as the excitation sources for the Raman measurements in this study. We chose a

laser power well below 2 mW to avoid any laser-induced heating effects during the measurements. For the Raman experiments, thick graphite flakes were used as the bottom layer in the encapsulated samples to avoid the background Raman spectrum of the Si/SiO₂ substrate.

TEM imaging. Aberration-corrected TEM, EDX spectroscopy and electron diffraction experiments were carried out using a JEOL ARM 200F TEM microscope operated at an operating voltage of 80 kV. The dose rate for high-resolution transmission electron microscope imaging was maintained at 10⁴ electrons per Å² per s. EDX spectroscopy was performed using the ARM's window-less Oxford Instruments X-MaxN 100TLE detector and TEM images were recorded using a Gatan Orius charge-coupled device camera.

An FEI Titan 80–200 ChemiSTEM equipped with probe-side aberration correction and an X-FEG electron source was used for the aberration-corrected scanning transmission electron microscope (STEM) imaging, EELS and electron diffraction analysis. STEM experiments were performed using an acceleration voltage of 200 kV, a beam current of 150 pA and a convergence angle of 21 mrad. EDX spectrum imaging was performed using the Titan's four detector Super-X spectrometer system, providing a solid angle of ≈ 0.7 sr. EELS data were acquired using a GIF Quantum ER Spectrometer, with an energy dispersion of 0.25 eV and a collection angle of 62 mrad, providing an effective energy resolution of 1.8 eV. In standard STEM imaging mode, the high-angle annular dark field collection angles were 62–142 mrad, while during spectrum imaging the high-angle annular dark field collection angles were 60–190 mrad. Electron diffraction patterns were acquired with a beam current of 2 nA and with an illuminated area on the specimen of ≈ 1 μm².

Data availability. The data that support the findings of this study are available from the corresponding author on request.

References

- Geim, A. K. & Grigorieva, I. V. Van der Waals heterostructures. *Nature* **499**, 419–425 (2013).
- Gao, G. *et al.* Artificially stacked atomic layers: toward new van der Waals solids. *Nano Lett.* **12**, 3518–3525 (2012).
- Withers, F. *et al.* Light-emitting diodes by band-structure engineering in van der Waals heterostructures. *Nat. Mater.* **14**, 301–306 (2015).
- Mishchenko, A. *et al.* Twist-controlled resonant tunnelling in graphene/boron nitride/graphene heterostructures. *Nat. Nanotechnol.* **9**, 808–813 (2014).
- Haigh, S. J. *et al.* Cross-sectional imaging of individual layers and buried interfaces of graphene-based heterostructures and superlattices. *Nat. Mater.* **11**, 764–767 (2012).
- Algara-Siller, G. *et al.* Square ice in graphene nanocapillaries. *Nature* **519**, 443–445 (2015).
- Jiao, S. & Xu, Z. Water under the cover: structures and thermodynamics of water encapsulated by graphene. Preprint at <http://arxiv.org/abs/1509.07215> (2015).
- Aradhya, S. V., Frei, M., Hybertsen, M. S. & Venkataraman, L. Van der Waals interactions at metal/organic interfaces at the single-molecule level. *Nat. Mater.* **11**, 872–876 (2012).
- Rodriguez-Reyes, J. C. F. *et al.* Van der Waals interactions determine selectivity in catalysis by metallic gold. *J. Am. Chem. Soc.* **136**, 13333–13340 (2014).
- DelRio, F. W. *et al.* The role of van der Waals forces in adhesion of micromachined surfaces. *Nat. Mater.* **4**, 629–634 (2005).
- Lee, J. H. *et al.* Van der Waals force: a dominant factor for reactivity of graphene. *Nano Lett.* **15**, 319–325 (2015).
- Lim, C. H. *et al.* A hydrothermal anvil made of graphene nanobubbles on diamond. *Nat. Commun.* **4**, 1556 (2013).
- Lim, C. H. Y. X., Nesladek, M. & Loh, K. P. Observing high-pressure chemistry in graphene bubbles. *Angew. Chem. Int. Ed.* **53**, 215–219 (2014).
- Mu, R. *et al.* Visualizing chemical reactions confined under graphene. *Angew. Chem. Int. Ed.* **51**, 4856–4859 (2012).
- Sutter, P., Sadowski, J. T. & Sutter, E. A. Chemistry under cover: tuning metal-graphene interaction by reactive intercalation. *J. Am. Chem. Soc.* **132**, 8175–8179 (2010).
- Wojcik, M., Hauser, M., Li, W., Moon, S. & Xu, K. Graphene-enabled electron microscopy and correlated super-resolution microscopy of wet cells. *Nat. Commun.* **6**, 7384 (2015).
- Xu, K., Cao, P. & Heath, J. R. Graphene visualizes the first water adlayers on mica at ambient conditions. *Science* **329**, 1188–1191 (2010).
- Khestanova, E., Guinea, F., Fumagalli, L., Geim, A. K. & Grigorieva, I. V. Graphene bubbles on a substrate: universal shape and van der Waals pressure. Preprint at <https://arxiv.org/abs/1604.00086> (2016).
- Zamborlini, G. *et al.* Nanobubbles at GPa pressure under graphene. *Nano Lett.* **15**, 6162–6169 (2015).
- Littleford, R. E., Tackley, D. R., Cherryman, J. C., Dent, G. & Smith, W. E. A Raman and DFT study of substituted triphenylamines for use as charge transfer materials in light emitting polymers. *J. Mol. Struct.* **692**, 81–90 (2004).

21. Wu, J., Wang, H., Xu, S. & Xu, W. Comparison of shearing force and hydrostatic pressure on molecular structures of triphenylamine by fluorescence and Raman spectroscopies. *J. Phys. Chem. A* **119**, 1303–1308 (2015).
22. Bethell, D. E. & Sheppard, N. The infra-red spectrum and structure of boric acid. *Trans. Faraday Soc.* **51**, 9–15 (1955).
23. Kuznetsov, A. Y. *et al.* Pressure-induced chemical decomposition and structural changes of boric acid. *J. Phys. Chem. B* **110**, 13858–13865 (2006).
24. Boldyreva, E. & Dera, P. in *High-Pressure Crystallography: From Fundamental Phenomena to Technological Applications* (Springer, 2010).
25. Capwell, R. J. Raman spectra of crystalline and molten MgCl_2 . *Chem. Phys. Lett.* **12**, 443–446 (1972).
26. Voigt, W. & Klaeboe, P. Raman spectroscopic evidence for cation-anion contact in molten hydrates of magnesium chloride. *Acta Chem. Scand.* **A40**, 354–357 (1986).
27. Manson, N. B., Von der Ohe, W. & Chodos, S. L. Second-order Raman spectrum of MgO . *Phys. Rev. B* **3**, 1968–1972 (1971).
28. Billat, A., Mon, J. P. & Voisin, M. Experimental and theoretical study of Raman scattering in Co^{++} - and Fe^{++} -doped magnesium oxide. *Phys. Status Solidi B* **67**, 335–343 (1975).
29. Marshall, W. L. & Franck, E. U. Ion product of water substance, 0–1,000 °C, 1–10,000 bars new international formulation and its background. *J. Phys. Chem. Ref. Data* **10**, 295–304 (1981).
30. Ding, Y. *et al.* Nanoscale magnesium hydroxide and magnesium oxide powders: control over size, shape, and structure via hydrothermal synthesis. *Chem. Mater.* **13**, 435–440 (2001).
31. Komatsu, K. *et al.* Crystal structure of magnesium dichloride decahydrate determined by X-ray and neutron diffraction under high pressure. *Acta Crystallogr. B Struct. Eng. Mater.* **B71**, 74–80 (2015).
32. Kruger, M. B., Williams, Q. & Jeanloz, R. Vibrational spectra of $\text{Mg}(\text{OH})_2$ and $\text{Ca}(\text{OH})_2$ under pressure. *J. Chem. Phys.* **91**, 5910–5915 (1989).
33. Malone, L. J. & Dolter, T. O. *Basic Concepts of Chemistry* 9th edn (Wiley, 2012).
34. Nair, R. R. *et al.* Graphene as a transparent conductive support for studying biological molecules by transmission electron microscopy. *Appl. Phys. Lett.* **97**, 153102 (2010).
35. Novoselov, K. S. *et al.* Two-dimensional atomic crystals. *Proc. Natl Acad. Sci. USA* **102**, 10451–10453 (2005).
36. Ferrari, A. C. *et al.* Raman spectrum of graphene and graphene layers. *Phys. Rev. Lett.* **97**, 187401 (2006).
37. Kretinin, A. V. *et al.* Electronic properties of graphene encapsulated with different two-dimensional atomic crystals. *Nano Lett.* **14**, 3270–3276 (2014).
38. Algara-Siller, G., Lehtinen, O., Turchanin, A. & Kaiser, U. Dry-cleaning of graphene. *Appl. Phys. Lett.* **104**, 153115 (2014).

Acknowledgements

This work was supported by the Royal Society and the Engineering and Physical Sciences Research Council, UK (EP/K016946/1). S.J.H. and E.P. acknowledge support from the Defense Threat Reduction Agency (HDTRA-12-01-0013). This work was also supported by SuperSTEM: the U.K.'s National Facility for aberration corrected STEM funded by the Engineering and Physical Sciences Research Council.

Author contributions

R.R.N. designed the project and directed it with help from K.S.V.; K.S.V. prepared the samples, performed the measurements and carried out data analysis; E.P., J.A., R.J.K., J.S. and S.J.H. carried out electron microscopy measurements and data analysis; J.D., J.B., P.C. and M.N.-A. carried out DFT calculations and molecular dynamic simulations; A.K.G. participated in discussions and project design; R.R.N., K.S.V. and A.K.G. wrote the manuscript. All authors contributed to discussions.

Additional information

Supplementary Information accompanies this paper at <http://www.nature.com/naturecommunications>

Competing financial interests: The authors declare no competing financial interests.

Reprints and permission information is available online at <http://npng.nature.com/reprintsandpermissions/>

How to cite this article: Vasu, K. S. *et al.* Van der Waals pressure and its effect on trapped interlayer molecules. *Nat. Commun.* 7:12168 doi: 10.1038/ncomms12168 (2016).



This work is licensed under a Creative Commons Attribution 4.0 International License. The images or other third party material in this article are included in the article's Creative Commons license, unless indicated otherwise in the credit line; if the material is not included under the Creative Commons license, users will need to obtain permission from the license holder to reproduce the material. To view a copy of this license, visit <http://creativecommons.org/licenses/by/4.0/>

© The Author(s) 2016